Microstructural analysis and mechanical behaviour of oxide/oxide cmcs prepared by continuous tow impregnation

Zoé Borius, A. Débarre, M. Singlard, Thierry Cutard, Aurélie Julian-Jankowiak

MICROSTRUCTURAL ANALYSIS AND MECHANICAL BEHAVIOUR OF OXIDE/OXIDE CMCS PREPARED BY CONTINUOUS TOW IMPREGNATION

Z. Borius[1, 2, 3], A. Debarre[1], M. Singlard[2], T. Cutard[3] and A. Julian-Jankowiak[1]

[1]ONERA, DMAS, Université Paris-Saclay, F-92322 Châtillon, France
[2]IRT Saint-Exupéry, F-33405 Talence, France
[3]ICA, Université de Toulouse, CNRS, IMT Mines Albi, INSA, ISAE-SUPAERO, UPS, Campus Jarlard, F-81013 Albi, France

Keywords: Ceramic Matrix Composite, boehmite, microstructure, tensile tests, bending tests

Abstract
This paper focuses on the analysis of the mechanical behaviour of alumina/alumina ceramic matrix composites (CMCs) developed by a continuous tow impregnation method, in relation to their microstructures. The influence of the aqueous slurry formulation on the microstructures of the materials and their tensile and bending properties is studied. A combination of a hygroscopic plasticizer (glycerol) and a gelling powder (boehmite) within the slurry is needed to obtain a good interply cohesion in the composite. A large amount of glycerol (20 wt.% relative to the alumina mass) allows a fine-scale porosity distributed throughout the matrix with few large pores which allows to reach a high Young's, around 130 – 150 GPa. Moreover, reducing the plasticizer amount induces the apparition of delaminations and defects appear the microstructure, hence decreasing the stiffness. Then, increasing the boehmite amount (from 5 wt.% to 10 wt.%), the damage tolerance is enhanced, likely due to a higher densification level induced by the presence of the boehmite powder.

1. Introduction

Oxide/oxide ceramic matrix composites (CMCs) are being explored for continuous thermomechanical applications within the temperature range of 800 to 1000 °C, under moderate mechanical loads. They could allow both the required increase in operating temperatures in aeronautical propulsion systems and a weight reduction, due to their low density. In particular, oxide/oxide CMCs stand out for their ability to operate in oxidising atmospheres without the need for fibre coating. One of the main challenges of these recent materials is to automate their production processes and to control their heterogeneous microstructures and properties.

Since fibres provide the mechanical resistance of composites, it is necessary to avoid the propagation of matrix cracks through the fibres in order to induce a certain damage tolerance behaviour. It can be realized through two methods: introducing a weak interface between the fibres and the matrix, or employing a weak matrix, which is characterized by controlled and fine-scale porosity [1]. In particular, the weak matrix concept is interesting for oxide/oxide CMCs, as the fibres are resistant to oxidation [1–3]. A high porosity level matrix (~30-40 vol.%) [4] results in a matrix with low fracture toughness in which crack deflection is favoured, leading to non-simultaneous fibre failures.

The elaboration process of oxide/oxide CMCs usually includes liquid impregnation of the fibres with an aqueous slurry. Conventionally, a 2D fibre fabric is used for impregnation, then comes a shaping and drying step, followed by a high temperature sintering [5–8]. A partial sintering is prefered in order to prevent complete densification of the matrix and hence, maintain a high level of porosity. However,

these processes are non-automated and costly, particularly regarding fibres, which account for up to 70 % of the raw material cost [9].

A significant cost reduction approach is the use of fibre tows instead of fibre fabrics, as it eliminates the need for weaving. Also tows with higher filament counts are now available and less expensive. Coupled with Automated Fibre Placement (AFP), it enables both the reduction of the fibre costs, and the manufacturing of complex parts [10]. Very few studies focused on this method for oxide/oxide CMCs. Indeed, 3M is the only company providing an experimental product that is an impregnated tow (tow-preg) with Nextel^{TM}610 spread tow impregnated with an aqueous alumina slurry.

The present work involves developing alumina/alumina CMCs through a continuous fibre tow impregnation process with an aqueous slurry, and to study the mechanical behaviour of the obtained CMCs, in relation to their microstructures. Thus, the influence of the slurry composition on the microstructures and the mechanical properties of alumina/alumina composites has been evaluated. The spatial distribution of pores was studied through X-ray tomography and scanning electron microscopy (SEM) observations. The mechanical behaviour of CMCs plates was characterized at room temperature with both four-point bending and tensile tests.

2. Materials and methods

2.1. Raw materials and slurries

Nextel^{TM} roving of alumina fibres N610 (20 000 denier, 3M, USA) with polyvinyl alcohol (PVA) coating was chosen as the fibre reinforcement. These fibres are pure α-alumina ones, with a filament diameter of 12 µm, a density of 3.9 g.cm^{-3} and a filament tensile modulus of 370 GPa. The tow has a nominal filament count of 5100, and a linear weight of 0.0022 kg.m^{-1}.

The high-purity α-alumina powder SM8 (Baïkowski, France, d_{50}=0.2 µm, S_{BET}=10 m^2.g^{-1}), was used as the raw oxide powder for the aqueous slurry in this study. Besides, a boehmite powder was also introduced as a gelling agent. The water dispersible boehmite Disperal P2 (Sasol, Germany) with a median granule size of 45 µm, a crystallite size of 4.5 nm and a specific surface area of 260 m^2.g^{-1} was used. During the sintering heat treatment, boehmite will undergo various transformations, and convert into α-alumina around 1200°C [11–13].

Regarding the organic additives, a polyvinyl alcohol-based binder Optapix PAF 35 (Zschimmer & Schwarz, Germany) was chosen. The amount of PVA was not studied in this study and the same ratio of PVA to alumina powder is conserved for all slurries. Glycerol (Sigma-Aldrich, USA), which is a highly hygroscopic plasticizer of the PVA, was added to the slurry in order to give to the impregnated tows sufficient powder hold, flexibility and tack for composite manufacturig.

Different slurries were formulated with various amounts of glycerol and boehmite powder (Table 1). The mass contents of plasticizer and boehmite powder are calculated as mass ratios to the alumina mass. First, a slurry containing only glycerol at 20 wt.% (G20) was formulated. B5G20 and B10G20 slurries contain the same amount of glycerol, and also 5 wt.% and 10 wt.% of boehmite powder, respectively. B10G10 contains 10 wt.% of boehmite and 10 wt.% of glycerol, in order to reduce organic content by replacing it with boehmite powder.

Table 1: Slurry formulations; $w_{plasticizer}$ and $w_{boehmite}$ are the mass ratios (in wt.%) to the alumina mass of plasticizer and boehmite powder, respectively.

Slurry	*G20*	*B5G20*	*B10G20*	*B10G10*
$w_{plasticizer}$	20	20	20	10
$w_{boehmite}$	0	5	10	10

2.2. Manufacturing process

The automated impregnation line (Huguet Ingénierie, France) used for tow impregnation in this work is depicted

Figure 1. Initially, the tow extracted from the as-received roving is unwound and directed into a tubular furnace to remove fibre sizing. Then, the cleaned tow is spread out by multiple rollers before the impregnation bath, which is a metal container filled with the slurry. Afterward, the impregnated tow undergoes drying in a convective heating furnace with forced airflow to evaporate the water content from the impregnated slurry. The tow then passes through a series of rollers (tractor) to regulate speed throughout the line. Finally, at the end of the line, the dried tow is wound onto a mandrel, resulting in a product called "tow-preg". Several parameters can be monitored on the impregnation line, such as tension, roving speed, drying temperature and air flow. The processing speed was set at 0.5 m.min^{-1}, and the tension at 8 N. The drying parameters were optimized depending on the drying behaviour of each tested slurry. A square mandrel with sides of 125 mm was chosen to obtain unidirectional plies.

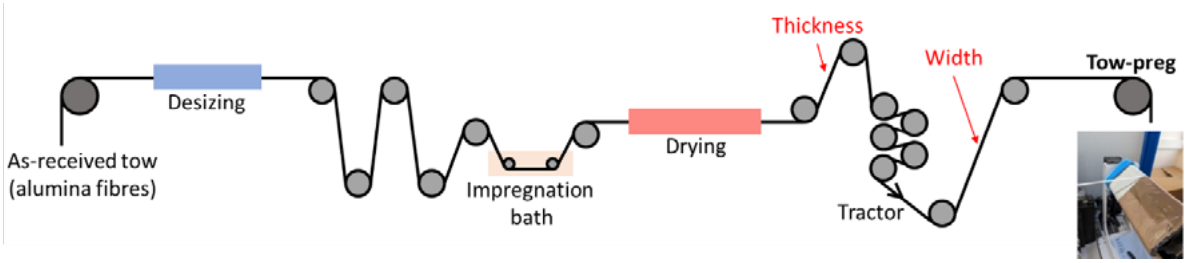

Figure 1: Schematic view of the impregnation line.

The plies are moisture-conditioned at RH=85% to reactivate a certain tack thanks to the presence of hygroscopic plasticizers. Then, they are layered to form a symmetric $[0/90/0/90]_s$ laminated composite plate and placed into an autoclave. Temperature-vacuum-pressure cycles in the autoclave were defined for each organic plasticizer, which are present in large quantities in tow-pregs. The aim is to initiate their degradation slowly while increasing the vacuum level simultaneously, to limit the volume of gas produced during their pyrolysis [13]. An isothermal dwell is then maintained to complete degradation. Finally, a partial sintering at 1200°C is applied so as to keep a high porosity level within the matrix.

2.3. Microstructural characterisations

The porosity of the as-processed composite plates was measured by the Archimede's method. The fibre volume content is then calculated, knowing the fibre length contained in the material, the linear density of the fibres, and the apparent density of the material.

Finally, the microstructure of materials is studied by scanning electron microscopy (SEM, MIRA TESCAN) and X-ray tomography (RX Solutions EasyTom 230) on cut samples of 20 x 20 mm^2. Then, the images from tomography were segmented using Otsu thresholding technique [14] to differentiate material and porosity areas, in order to determine a porosity level.

2.4. Mechanical characterisations

In-plane mechanical properties of the composites were studied through uniaxial monotonic tensile tests at room temperature, using a Z150 Zwick/Roell Materials testing machine. The tests were performed with a controlled displacement rate of 0.5 mm.min^{-1}. Straight-sided specimens, 120 mm x 16 mm x *composite thickness* with a gauge length of 50 mm were used. Pure aluminium annealed thin foils (0.2 mm thick) are used as tabs to ensure load transfer to the specimen, without damage. A two FLIR cameras system with a resolution of 9 MPx recorded the test at 5 Hz and the images are used to perform stereo digital image correlation (DIC, VIC-3D™). Acoustic activity such as matrix cracking or fibre failure is recorded during the test using a Nano03 sensor (Physical Acoustics Corporation).

Flexural strength was evaluated using four-point bending tests conducted using a Z010 Zwick machine (1 kN) running at a cross-head speed of 1 $mm.min^{-1}$ and with outer and inner spans of 64 and 32 mm, respectively. Straight-sided specimens, 75 mm x 13 mm x *composite thickness* were used. A LVDT sensor is in contact with the underside of the specimen, at its centre, to measure the maximum value of the deflection during the test. Only one previously described FLIR camera recorded the test at 5 Hz.

3. Results and discussion

3.1. Influence of slurry composition on the CMCs microstructures

The morphological characteristics of the 8 plies CMCs plates are summed up in Table 2. The CMC prepared with the glycerol-only slurry (G20) exhibits a high porosity level of 34 vol.%. Combining glycerol and boehmite powder allows to decrease the porosity level to 23-26 vol.%. Indeed, thanks to its gelling properties, the boehmite powder increases the tow-pregs tack when moisture-conditioned, and favours inter-ply cohesion, resulting in composites that are denser and with higher fibre volume fraction. Prabhakaran et al. [15] found out that boehmite acts not only as a binder in an aqueous alumina slurry, but also as a sintering aid, that could explain the reduction in porosity.

Table 2: Morphological characteristics of 8 plies CMCs plates.

Material	*G20*	*B5G20*	*B10G20*	*B10G10*
Porosity (vol.%)	34	23	23	26
Fibres (vol.%)	41	52	57	55
Thickness (mm)	2.49 ± 0.12	2.48 ± 0.13	2.00 ± 0.09	2.02 ± 0.10

The ability of boehmite powder to increase interply cohesion is confirmed by the microstructures of the materials, displayed in Figure 2. Indeed, large delaminations between plies without boehmite powder can be observed in G20 microstructure. These defects, measuring a few millimeters, explain the high porosity of G20 plate. For materials containing both glycerol and boehmite, no delamination was observed. However, B5G20 and B10G20 exhibit about the same pores distribution, with a strong inter-ply bonding, while B10G10 presents more porosity and cracks within the matrix.

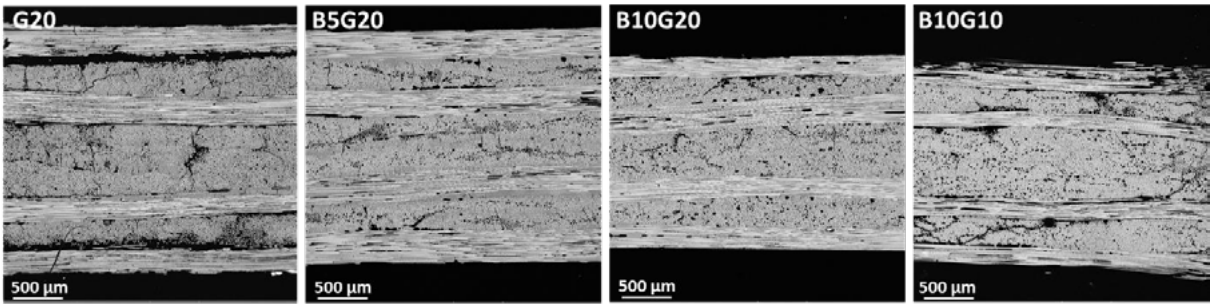

Figure 2: Microstructures of 8 plies CMC plates (SEM cross-sections).

Specimens of 20 x 20 mm^2 were cut for X-ray tomography analysis. Their porosities were measured with Archimede's method, to compare with the entire plates. The analysed area measures 20 mm^3 with a voxel size of 5 µm. The 2D porosity is detected (for pores larger than 25 μm^2) by image segmentation using Otsu thresholding method. Then, the porosity level in the volume of the specimen is calculated. As the pores are cylindrical, an ellipse is fitted around each pore, and the length of its largest dimension is extracted.

C. Ben Ramdane et al. [16] proposed a classification of the pores of 2D Nextel^{TM}610/alumina CMCs depending on their diameters, when considered spherical, into three domains: the macroporosity (diameter superior to 10 µm), the microporosity (diameter between 0.1 and 10 µm) and the nanoporosity

(diameter inferior to 0.1 µm). Nanopores are located within the matrix, micropores corresponds to small pores or microcracks, and macropores are located between plies or inside a ply, and can be prejudicial for the mechanical resistance of the composite. They studied the pore size distribution by mercury intrusion porosimetry, assuming pores are spherical. They concluded that the nanoporosity is the most significant, constituting 13 % of the total 25 % porosity measured by Archimed's method. In our work, the X-ray tomography analysis does not detect the micro or nanoporosity, but they are included in the total porosity measured by Archimede's method as well.

Table 3 sums up the total porosity of the specimens measured with Archimede's method, as well as the macroporosity volume fraction and the number of macropores determined by images segmentation from X-ray tomography. All specimens exhibit a porosity very close to that of the whole plates. Although the specimens B5G20, B10G20, and B10G10 have the same total porosity, they have different pore size distribution. B10G10 exhibits a higher amount of macropores (7.4 vol.%) compared to the two other compositions (4 – 5 vol.%), and a smaller number of detected pores. Hence, B10G10 contains both more large sized pores, and less fine porosity within the matrix. Figure 3 displays a view of the detected macropores and their largest dimension distribution for the composition B5G20. For all samples, the pores are cylindrical and along the fibres. Moreover, some delaminations can be observed for B10G10 composition when visualising the 3D pores distribution. SEM images reveal finer pores within the matrix on the cross section, while X-ray tomography images allow to depict the macropores in 3D.

Table 3: Porosity analysis of 20 x 20 mm^2 specimens. The total porosity is measured by Archimede's method, the macropores are detected by X-ray tomography images segmentation.

Specimens	*B5G20*	*B10G20*	*B10G10*
Total porosity (vol.%)	22	22	22
Macroporosity (vol.%)	4.3	4.9	7.4
Number of macropores (x 10^6)	3.1	3.0	2.4

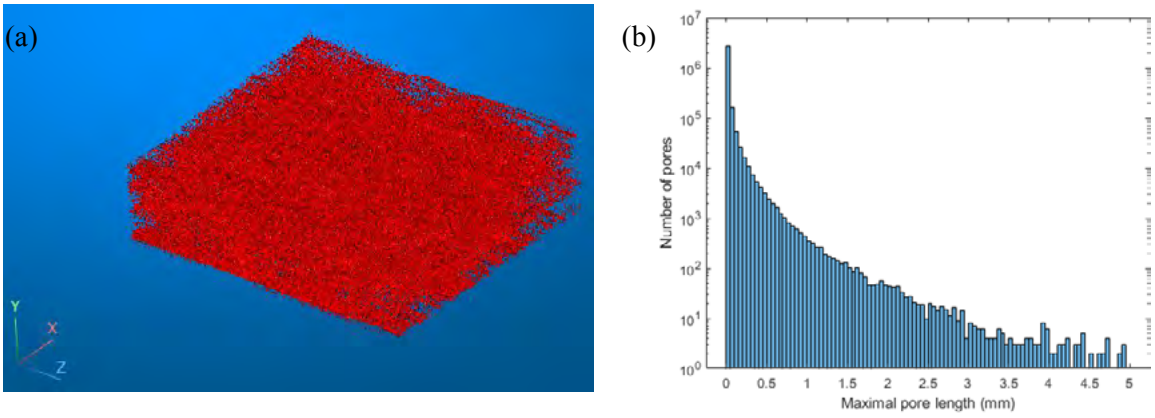

Figure 3: X-ray tomography pores visualisation (a) and distribution (b) for a 20 x 20 x *thickness* mm^3 B5G20 specimen.

3.2. Study of the mechanical behaviour of CMCs in relation to their microstructures

Tensile and four-points bending tests were conducted on at least 3 specimens per composition. Their porosities have been measured, and the results on the cut specimens were similar the those carried out on the whole plates (Table 2). Figure 4 illustrates a representative stress-strain curve for each composition, while Table 4 sums up the following mechanical properties: stiffness, stress and strain at failure (σ_f and ε_f).

With 20 wt.% of glycerol, when raising the boehmite content, the stiffness remains the same while damage tolerance increases, highlighted by higher stress and strain values at failure in both tensile and bending tests. Indeed, B5G20 exhibits a tensile failure stress $\sigma_f = 197 \pm 9$ MPa and a tensile fracture strain $\varepsilon_f = 0.17 \pm 0.01$ % while the values for B10G20 increase up to $\sigma_f = 266 \pm 36$ MPa and $\varepsilon_f = 0.28 \pm 0.06$ %. The Young's modulus E is not affected by the difference in fibre volume fraction between B5G20, that has 52 vol.% fibres and B10G20, that has a higher fibre volume fraction of 57 vol.%. Their total porosities as well as their pores distributions are equivalent.
On the contrary, when reducing the glycerol content, the stiffness drops: from 115 ± 7 GPa to 94 ± 13 GPa for tensile tests, and from 149 ± 8 GPa to 134 ± 9 GPa for bending tests. The failure stress and strain in tensile tests are reduced by 22 % and 8 % respectively, while they drop more drastically in bending tests: they are reduced by 57 % and 39 % respectively.

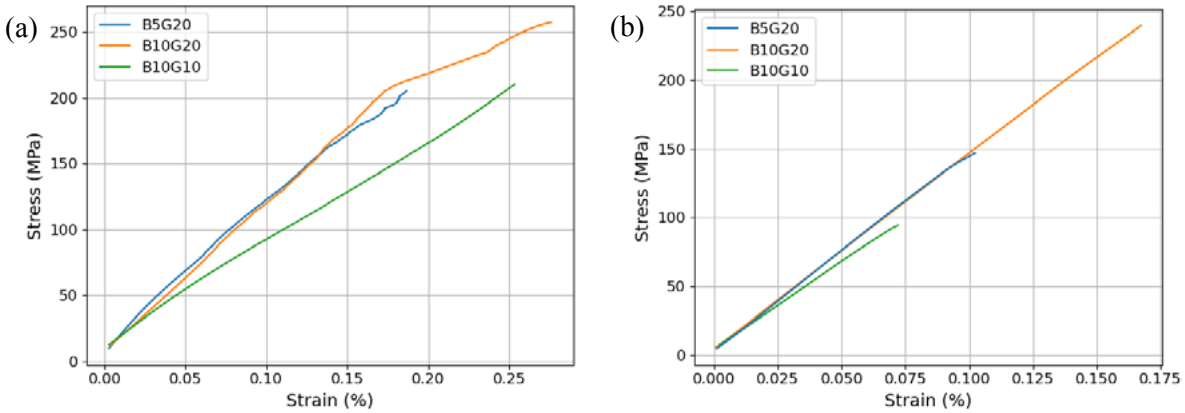

Figure 4: Mechanical behaviour of CMCs: (a) in tensile testing and (b) in four-points bending testing.

Table 4: Mechanical properties of the tested CMCs.

Material	*B5G20*	*B10G20*	*B10G10*
Tensile E (GPa)	126 ± 16	115 ± 7	94 ± 13
Tensile σ_f (MPa)	197 ± 9	266 ± 36	207 ± 27
Tensile ε_f (%)	0.171 ± 0.014	0.281 ± 0.055	0.259 ± 0.033
Bending E (GPa)	150 ± 5	149 ± 8	134 ± 9
Bending σ_b (MPa)	147 ± 36	238 ± 29	103 ± 25
Bending ε_b (%)	0.098 ± 0.020	0.161 ± 0.019	0.099 ± 0.034

For a 12 plies composite 2D Nextel^{TM}610/alumina under tensile loading, with 49 % fibres and 24 % porosity, C. Ben Ramdane et al. [16] measured a failure stress of 260 ± 37 MPa, a failure strain of 0.30 ± 0.09 % and an elastic modulus of 134 ± 19 GPa. The values obtained in this work for B10G20 composition are similar. Nevertheless, the two materials are different: ours consists of the layering of 8 unidirectionnal plies while the 2D Nextel^{TM}610/alumina composite is made of 12 2D plies. The fibre fraction volume for the 2D fabric composite is lower (49 vol.% versus 57 vol.%), and because of the weaving we can assume that the proportion of the fibres in the loading direction is even smaller. Under bending loading, A. Debarre et al. [7] observed for the 2D Nextel^{TM}610/alumina a quasi-linear behaviour as well. They measured higher failure resistance: 337 ± 57 MPa for the stress, and 0.29 ± 0.06 % for the strain, that could be due to the 2D structure of each ply, that creates a stronger bond between the fibres at 0° and 90°. In our case, the 0° and 90° fibres are only bonded by the matrix, which may reduce the interply shear strength.

The damage tolerance of the CMCs is evident when looking at the tensile stress-strain curve, as a change in the slope of the behaviour curve is observed (Figure 4 (a)). For bending tests, the behaviour appears

more linear (Figure 4 (b)). However, damage before the total failure of the material can be highlighted by focusing on acoustic events register throughout the test. Figure 5 displays the cumulative energy of acoustic events registered during bending testing for B5G20 and B10G10 CMCs only (as B10G20 presents the same behaviour than B5G20). The cumulative energy starts to increase at a stress value of 20 MPa that represents the first matrix cracks, which do not affect the mechanical strength of the materials. After this damage threshold, the energy gradually increases as both stress and strain rise. For B5G20, a jump in energy is observed at $\sigma = 140$ MPa, that corresponds to a significant crack of the matrix or several fibres breaks, which implies a load transfer to the fibres. Both the strain and stress continue to increase after this event, thus revealing the damage tolerance behaviour. This phenomenon is also revealed by looking at the images of the specimen's cross-sections taken from the FLIR camera during the test. Some cracks initiation and propagation in the matrix can be observed for B5G20 and B10G20, while the load continues to increase, until inter-ply delamination or multiple fibre failure occur, leading to a drop in stress and thus the failure of the CMC. Similar observations were made by C. Ben Ramdane et al. [16] when studying the acoustic emission of an 2D Nextel^{TM}610/alumina CMC through tensile/compression testing. They determined a higher damage threshold of 48 MPa. If the loading is below this value, the acoustic activity is negligible. The quasi-linear segment in their strain-stress curves corresponds to a small and regular activity, afterwards the activity increases due to fibre failures, up to the final CMC failure. In the case of B10G10, the jump in the cumulative energy occurs at the same time as the failure of the material, showing a brittle behaviour. This, as well as the drop in bending properties for B10G10, could be explained by the fact that in bending tests, the loaded section is smaller than in tensile tests, and the presence of delaminations (seen in B10G10 microstructure) in this section would result in early and more brittle material failure.

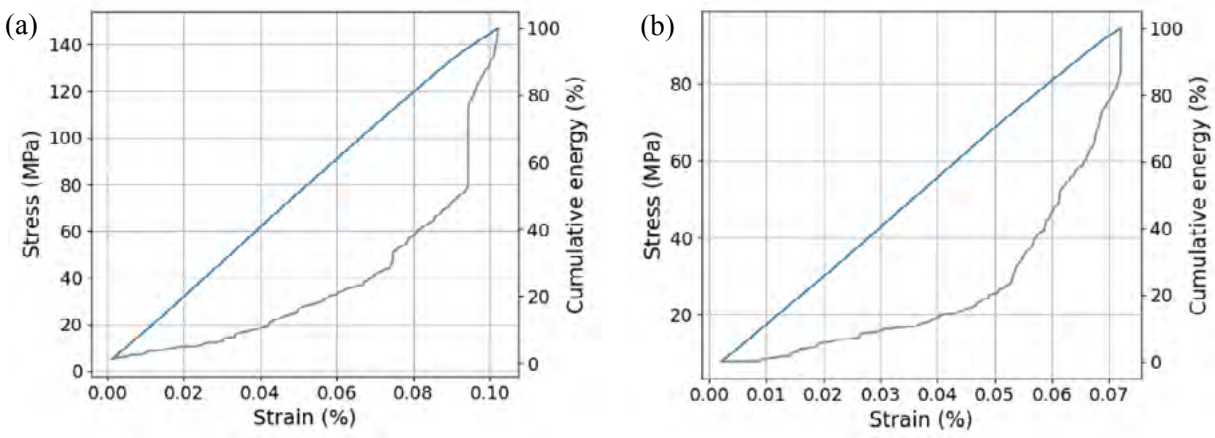

Figure 5: Acoustic activity registered during four-points bending tests of: (a) B5G20 and (b) B10G10 CMCs. (Blue: stress and grey: cumulative energy).

3. Conclusions

The manufacturing of oxide/oxide CMCs by continuous tow impregnation offers a cost reduction and a process automation that could limit heterogeneities in theses materials' microstructures. However, it requires a slurry that provides impregnated tows with sufficient flexibility and tackiness to produce composites. In this work, a combination of a hygroscopic plasticizer, glycerol and a gelling powder of boehmite, in an aqueous alumina slurry was found to be suitable for achieving interply cohesion.

A large amount of glycerol (20 wt.% relative to the alumina mass) results in a CMC with a fine-scale porosity distributed throughout the matrix with few large pores. This type of CMC microstructure ensures a damage tolerance behaviour, and a high Young's modulus, around 130 – 150 GPa. Moreover, reducing the plasticizer amount induces the apparition of delaminations and defects in the microstructure, hence decreasing the CMC stiffness. Also, it reduces damage tolerance and results in a more fragile fracture. Finally, when the boehmite amount is increased from 5 wt.% to 10 wt.%, the CMC

damage tolerance is enhanced, likely due to a higher densification level induced by the introduction of the boehmite powder.

Acknowledgments
The authors would like to thank Katia Dennis for her assistance with samples preparation, Anne Mavel, Céline Le Sinq and Sarah Boukobza for conducting the mechanical tests and Frédéric Laurin for his help with X-ray tomography images analysis.

References
[1] Zok FW, Levi CG. Mechanical Properties of Porous-Matrix Ceramic Composites. Adv Eng Mater 2001:9. https://doi.org/10.1002/1527-2648(200101)3:1/2<15::AID-ADEM15>3.0.CO;2-A.
[2] Mechnich P, Welter M. Porous Oxide Ceramic Matrix Composites – Properties, Manufacturing, and Applications. Encycl. Mater. Compos., Elsevier; 2021, p. 48–54. https://doi.org/10.1016/B978-0-12-819724-0.00073-2.
[3] Simon RA. Progress in Processing and Performance of Porous-Matrix Oxide/Oxide Composites. Int J Appl Ceram Technol 2005;2:9. https://doi.org/10.1111/j.1744-7402.2005.02016.x.
[4] Mattoni MA, Yang JY, Levi CG, Zok FW. Effects of Matrix Porosity on the Mechanical Properties of a Porous-Matrix, All-Oxide Ceramic Composite. J Am Ceram Soc 2001;84:9. https://doi.org/10.1111/j.1151-2916.2001.tb01059.x.
[5] Guglielmi PO, Nunes GF, Hablitzel M, Hotza D, Janssen R. Production of Oxide Ceramic Matrix Composites by a Prepreg Technique. Mater Sci Forum 2012;727–728:556–61. https://doi.org/10.4028/www.scientific.net/MSF.727-728.556.
[6] Ben Ramdane C. Etude et modélisation du comportement mécanique de CMC oxyde/oxyde. Université de Bordeaux, 2014.
[7] Debarre A. Comportement mécanique à haute température d'un composite alumine/alumine. Université PSL, 2021.
[8] Puchas G, Möckel S, Krenkel W. Novel prepreg manufacturing process for oxide fiber composites. J Eur Ceram Soc 2020;40:5930–41. https://doi.org/10.1016/j.jeurceramsoc.2020.06.064.
[9] Pritzkow WEC, Almeida RSM, Mateus LB, Tushtev K, Rezwan K. All-oxide ceramic matrix composites (OCMC) based on low cost 3M Nextel™ 610 fabrics. J Eur Ceram Soc 2021;41:3177–87. https://doi.org/10.1016/j.jeurceramsoc.2020.05.070.
[10] Arrabiyeh PA, May D, Eckrich M, Dlugaj AM. An overview on current manufacturing technologies: Processing continuous rovings impregnated with thermoset resin. Polym Compos 2021;42:5630–55. https://doi.org/10.1002/pc.26274.
[11] Ananthakumar S, Menon ARR, Prabhakaran K, Warrier KGK. Rheology and packing characteristics of alumina extrusion using boehmite gel as a binder. Ceram Int 2001;27:231–7. https://doi.org/10.1016/S0272-8842(00)00070-5.
[12] Zargar HR, Fard FG, Rezaie HR. The influence of nano boehmite on spinel formation in the alumina-magnesia system at low temperatures. Journal of Ceramic Processing Research 2008;9:46–51.
[13] Borius Z, Débarre A, Singlard M, Cutard T, Julian-Jankowiak A. Impact of additives on the quality of oxide/oxide tow-pregs obtained by continuous fibre impregnation. Compos Part Appl Sci Manuf 2024;184:108238. https://doi.org/10.1016/j.compositesa.2024.108238.
[14] Otsu N. A Threshold Selection Method from Gray-Level Histograms. IEEE Trans Syst Man Cybern 1979;9:62–6. https://doi.org/10.1109/TSMC.1979.4310076.
[15] Prabhakaran K, Ananthakumar S, Pavithran C. Gel Casting of Alumina using Boehmite as a Binder. J Eur Ceram Soc 1999;19:2875–81. https://doi.org/10.1016/S0955-2219(99)00075-8.
[16] Ben Ramdane C, Julian-Jankowiak A, Valle R, Renollet Y, Parlier M, Martin E, et al. Microstructure and mechanical behaviour of a Nextel™610/alumina weak matrix composite subjected to tensile and compressive loadings. J Eur Ceram Soc 2017;37:2919–32. https://doi.org/10.1016/j.jeurceramsoc.2017.02.042.